Resonance Electromagnetic Absorption by Nonspherical Dielectric Objects

PETER W. BARBER, MEMBER, IEEE

Abstract—**The extended boundary condition method (EBCM) is used to develop a theoretical solution for the internal fields of isotropic and homogeneous nonspherical dielectric objects. The formulation is particularly effective for resonance-sized bodies. The computational capabilities of the technique are demonstrated by presenting numerical calculations of absorption efficiency versus electrical size (*ka*) and internal-field distributions at resonance for a number of lossy axisymmetric objects including spheres, spheroids, and a finite cylinder. The numerical limitations are discussed and a method is given which allows extension of the numerical technique to a larger class of problems.**

I. Introduction

THERE is currently a great interest in the scattering and absorption characteristics of dielectric objects. This interest is the result of a variety of new and diverse problems involving the interaction of electromagnetic (EM) waves with closed dielectric bodies. These studies include a determination of the power-absorption characteristics of man due to exposure to EM waves [1], the absorption and scattering of microwaves by raindrops [2], the design of miniature microwave filters using resonant spheres [3], and continuing investigations to apply laser light-scattering techniques to problems in microbiology [4]. In all of these studies a theoretical solution which describes the EM interaction is crucial. For spherical objects the Mie theory is used, while for other geometries it is necessary to employ alternate techniques, and these generally involve approximations with limited range of applicability, e.g., low *ka*, small deviation from spherical shape, etc. The need for new methods of analysis which will provide quantitative results and also increase our understanding of the interaction mechanisms, especially techniques suitable for nonspherical objects on the order of a wavelength in size (resonance-sized objects), is clearly indicated. Recent theoretical advances in this area have included a study of the resonance behavior of very high permittivity dielectrics [5], [6] and the solution of the vector wave equation in spheroidal coordinates [7].

A powerful technique for analyzing the interaction of electromagnetic waves with closed three-dimensional bodies has been developed by Waterman and is summarized in [8]. This technique, called the extended boundary condition method (EBCM), is ideally suited to investigating the resonance-region scattering and absorption characteristics of arbitrary-shaped dielectric objects. Furthermore, the theory is also applicable to an arbitrary number of bodies and to layered bodies [9], [10].

An alternative development of the EBCM has recently been given and has been applied to an investigation of the differential scattering characteristics of arbitrary-shaped dielectric bodies [11]. In the present paper, the EBCM is applied to the internal problem and we look at the case where the dielectric object is homogeneous, isotropic, and lossy, i.e., the dielectric constant is complex. This is a model which is useful in studies of EM absorption by man and raindrops and resonance characteristics of microwave resonators. It should be pointed out that although the absorption cross section and absorption efficiency can be determined independently from the scattering cross section by the forward amplitude theorem [12], the absorption problem must be solved separately if one requires detailed knowledge of the internal or surface-field distribution as well as total absorption.

The analysis begins with the development of the EBCM as it applies to the internal problem. The application of the extended boundary condition method to the internal-field problem closely follows the development which has previously been given for the dielectric-scattering problem. Therefore, only the highlights of the theory will be given here and the interested reader is referred to a previous paper [11].

The overall goal is to determine the internal field when an arbitrary dielectric body is illuminated by a plane electromagnetic wave. The dielectric body, assumed homogeneous and isotropic, is characterized by the constitutive parameters μ and ε, where ε may be complex, to describe a lossy material, and the surrounding medium is considered to be free space with parameters μ_0,ε_0. The problem is illustrated schematically in Fig. 1. We call this the complete problem to distinguish it from a special problem which will be constructed to aid in the solution. The total field everywhere is given by the sum of the incident field and the scattered field, where the incident field $\boldsymbol{E}^i,\boldsymbol{H}^i$ is the field present in the absence of the scatterer, and the scattered field $\boldsymbol{E}^s,\boldsymbol{H}^s$ is given by the difference between the field with the object present $(\boldsymbol{E},\boldsymbol{H})$ and the incident field; that is,

$$\boldsymbol{E}^s = \boldsymbol{E} - \boldsymbol{E}^i \quad \boldsymbol{H}^s = \boldsymbol{H} - \boldsymbol{H}^i.$$

This scattered field can be thought of as the field produced by polarization currents within the object.

We wish to solve for the total field $(\boldsymbol{E},\boldsymbol{H})$ within the dielectric body. To accomplish this, we begin by applying

Manuscript received April 23, 1976; revised September 7, 1976. This work was supported by the National Science Foundation under Grant GK 43124.

The author is with the Department of Bioengineering, University of Utah, Salt Lake City, UT 84112.

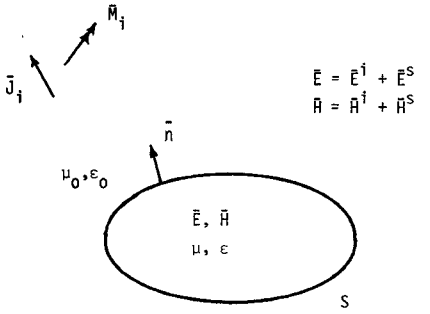

Fig. 1. The complete electromagnetic problem. J_i and M_i are the sources of the incident field. (Overbars in figs. appear boldface in text.)

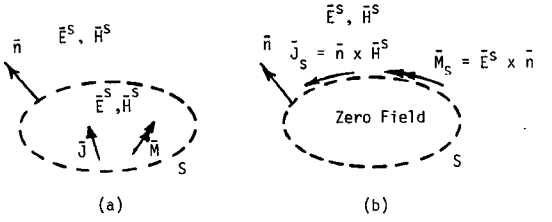

Fig. 2. Application of the equivalence theorem to the scattered-field sources.

the equivalence principle to construct a special problem which is used as an aid in solving the complete problem. Analyzing this special problem (which is identical to the problem of scattering by a perfect conductor), we write an expression for the scattered field in terms of tangential fields (currents) over a surface corresponding to the surface of the object. At this point, both the scattered field and the surface currents are unknown. We then obtain a relationship between the scattered field and the known incident field (by virtue of the fact that they must cancel each other in the interior of the special problem) and solve with the previously obtained expression to write the surface tangential fields in terms of the incident field. Returning then to the complete problem, we realize that the surface fields can also be written in terms of the internal field, thereby providing a relationship between the internal field and the incident field.

The general applicability of the method is demonstrated by making numerical calculations of the absorption efficiency and internal-field distributions at resonance for a variety of lossy dielectric bodies, including spheres, spheroids, and a finite cylinder. The numerical limitations are discussed and a method is given which allows extension of the numerical technique to a larger class of problems.

II. Analysis of the Special Problem

Consider a closed surface S which separates an isotropic homogenous medium into two regions as shown in Fig. 2(a). All the sources are contained within S so that the region outside S is source-free. Schelkunoff's equivalence theorem [13] states that the field in a source-free region bounded by a surface S could be produced by a distribution of electric and magnetic currents on this surface and, in

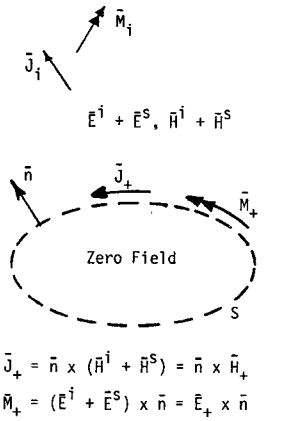

Fig. 3. The special problem which has been constructed to aid in the solution of the original problem. E_+ and H_+ are the external fields evaluated at the surface.

this sense, the actual source distribution can be replaced by an equivalent distribution. Furthermore, if the field produced by the original source is E^s,H^s, then the equivalent sources on S consist of an electric-current sheet of density $n \times H^s$ and a magnetic-current sheet of density $E^s \times n$, where the normal n points from the region containing the sources to the source-free region. The application of Schelkunoff's equivalence theorem is shown in Fig. 2(b). Note that the boundary conditions at S indicate that the surface currents produce a null field within S.

We relate the situation shown in Fig. 2 to the scattered-field portion of our problem by identifying J and M in Fig. 2(a) as polarization currents within S (which have been induced by an incident field), which radiate in free space to produce the scattered field E^s,H^s. In Fig. 2(b) these polarization currents have been replaced by equivalent surface currents which radiate the scattered field external to S and produce a null field inside S.

A similar procedure can be applied to the sources of the incident field and when combined with the equivalent problem which has been previously derived for the polarization currents and performing some additional transformations [11], we obtain the situation shown in Fig. 3.

It can be seen that external to the surface S, the sources and fields are exactly the same as those existing in the original problem and we have replaced the dielectric object by a set of surface currents over a surface S. Furthermore, these surface currents radiate in unbounded free space to produce the scattered field outside S and the negative of the incident field inside S. It should be emphasized that by using the equivalence theorem, we have created a special problem which, while related to the original problem, is merely an artifice which is useful in solving the original problem. An interesting observation is that this special problem, which is used to solve the dielectric EM problem, is, in fact, identical to the perfect conductor problem, i.e., the total field exists outside the body, with zero-field internal.

The entire region is unbounded and, therefore, the scattered fields everywhere due to the surface currents J_+ and M_+ can be determined via vector magnetic and electric

potentials [14]. In particular, the scattered electric field is given by

$$\boldsymbol{E}^s(\boldsymbol{r}) = \nabla \times \int_S (\boldsymbol{n} \times \boldsymbol{E}_+) g(kR)\, dS - \nabla \times \nabla \times \int_S \frac{1}{j\omega\varepsilon_0} (\boldsymbol{n} \times \boldsymbol{H}_+) g(kR)\, dS \quad (1)$$

where $g(kR)$ is the free-space Green's function $e^{jkR}/4\pi R$; $R = |\boldsymbol{r} - \boldsymbol{r}'|$; $\boldsymbol{r}'$ and $\boldsymbol{r}$ are position vectors from an interior origin to source and field points, respectively; and $k = 2\pi/\lambda$. An $e^{-j\omega t}$ time variation has been chosen to conform to previous EBCM developments [8]–[11]. The total field is then given by

$$\left.\begin{matrix}\boldsymbol{E}(r) \\ 0\end{matrix}\right\} = \boldsymbol{E}^i(\boldsymbol{r}) + \nabla \times \int_S (\boldsymbol{n} \times \boldsymbol{E}_+) g(kR)\, dS - \nabla \times \nabla \times \int_S \frac{1}{j\omega\varepsilon_0} (\boldsymbol{n} \times \boldsymbol{H}_+) g(kR)\, dS, \quad r \begin{cases}\text{outside } S \\ \text{inside } S\end{cases} \quad (2)$$

With respect to the region inside S, the requirement that the scattered field must cancel the incident field throughout the interior volume gives us an important relationship between the surface tangential fields and the incident field.

$$\nabla \times \int_S (\boldsymbol{n} \times \boldsymbol{E}_+) g(kR)\, dS - \nabla \times \nabla \times \int_S \frac{1}{j\omega\varepsilon_0} (\boldsymbol{n} \times \boldsymbol{H}_+) g(kR)\, dS = -\boldsymbol{E}^i(\boldsymbol{r}). \quad (3)$$

This equation can be expanded in a form suitable for numerical processing by making use of the spherical vector harmonics $\boldsymbol{M}$ and $\boldsymbol{N}$ which have been defined by Stratton [15]. Using these spherical vector harmonics, the incident field is given by

$$\boldsymbol{E}^i(\boldsymbol{r}) = \sum_{\upsilon=1}^{\infty} D_\upsilon [a_\upsilon \boldsymbol{M}_\upsilon^1(k\boldsymbol{r}) + b_\upsilon \boldsymbol{N}_\upsilon^1(k\boldsymbol{r})] \quad (4)$$

where υ is a combined index incorporating the spherical harmonic indices σ, m, and n. D_υ is a normalization constant and the expansion coefficients a_υ and b_υ are assumed known for a specified incident field. The superscript 1 on $\boldsymbol{M}$ and $\boldsymbol{N}$ indicates that these functions are of the type which are finite at the origin. The terms in the integrals of (3) are expanded as follows:

$$(\boldsymbol{n} \times \boldsymbol{E}_+) g(kR) = (\boldsymbol{n} \times \boldsymbol{E}_+) \cdot \bar{\boldsymbol{G}} \quad (5a)$$

$$(\boldsymbol{n} \times \boldsymbol{H}_+) g(kR) = (\boldsymbol{n} \times \boldsymbol{H}_+) \cdot \bar{\boldsymbol{G}} \quad (5b)$$

where $\bar{\boldsymbol{G}}(kR)$ is the free-space Green's dyadic given by Morse and Feshbach [16].

$$\bar{\boldsymbol{G}}(kR) = \frac{jk}{\pi} \sum_{\upsilon=1}^{\infty} D_\upsilon [\boldsymbol{M}_\upsilon^3(k\boldsymbol{r}_>) \boldsymbol{M}_\upsilon^1(k\boldsymbol{r}_<) + \boldsymbol{N}_\upsilon^3(k\boldsymbol{r}_>) \boldsymbol{N}_\upsilon^1(k\boldsymbol{r}_<)] \quad (6)$$

$\boldsymbol{r}_>, \boldsymbol{r}_<$ are, respectively, the greater and lesser of $\boldsymbol{r}, \boldsymbol{r}'$. The irrotational terms normally present in (6) are not specified, as they will be eliminated due to the curl operation in (3). $\boldsymbol{M}^1$ and $\boldsymbol{N}^1$ are functions finite at the origin, and $\boldsymbol{M}^3$ and $\boldsymbol{N}^3$ are functions representing outgoing waves.

Equation (3) is required to hold throughout the entire interior volume, i.e., for all r inside S. Equations (4)–(6) can now be substituted into (3), but before doing so, it should be pointed out that the Green's function expansion $g(kR) = e^{jkR}/4\pi R$ has a singularity at $R = 0$, i.e., for $\boldsymbol{r} = \boldsymbol{r}'$. Therefore, an expansion of (3) about an origin within the enclosed volume would appear to be valid only within an inscribed sphere rather than in the entire interior volume as required. This is true; however, it has been shown using analytical continuation arguments [8] that the solution of (3) within an inscribed sphere does, in fact, guarantee that the total field will be zero throughout the entire interior volume.

Substituting (4)–(6) into (3) gives the following set of equations for the surface currents in terms of the incident-field coefficients:

$$\frac{jk^2}{\pi} \int_S \left[\boldsymbol{N}_\upsilon^3(k\boldsymbol{r}') \cdot (\boldsymbol{n} \times \boldsymbol{E}_+) + j\left(\frac{\mu_0}{\varepsilon_0}\right)^{1/2} \boldsymbol{M}_\upsilon^3(k\boldsymbol{r}') \cdot (\boldsymbol{n} \times \boldsymbol{H}_+) \right] dS = -a_\upsilon \quad (7a)$$

$$\frac{jk^2}{\pi} \int_S \left[\boldsymbol{M}_\upsilon^3(k\boldsymbol{r}') \cdot (\boldsymbol{n} \times \boldsymbol{E}_+) + j\left(\frac{\mu_0}{\varepsilon_0}\right)^{1/2} \boldsymbol{N}_\upsilon^3(k\boldsymbol{r}') \cdot (\boldsymbol{n} \times \boldsymbol{H}_+) \right] dS = -b_\upsilon \quad (7b)$$

where $\varepsilon = 1,2,3,\cdots$. Note that the substitution into (3) has resulted in two sets of equations. The reason for this is that the coefficient of each regular wave function ($\boldsymbol{M}$ or $\boldsymbol{N}$) must vanish separately due to the orthogonality of the functions over a spherical surface about the origin. The solution of (7) guarantees that the total field will be zero throughout the entire interior volume.

III. The Complete Problem

Returning now to the original problem which we set out to solve, assume that the field inside the dielectric region can be represented by

$$\boldsymbol{E}(k'\boldsymbol{r}) = \sum_{\mu=1}^{N} [c_\mu \boldsymbol{M}_\mu^1(k'\boldsymbol{r}) + d_\mu \boldsymbol{N}_\mu^1(k'\boldsymbol{r})] \quad (8a)$$

where μ plays the same role as υ in (6) and c_μ and d_μ are unknown coefficients. $k' = \omega(\mu\varepsilon)^{1/2} = (\mu_r\varepsilon_r)^{1/2}k$. The $\boldsymbol{H}$-field internal to S is given by

$$\boldsymbol{H}(k'\boldsymbol{r}) = \frac{1}{j\omega\mu} (\nabla \times \boldsymbol{E}(k'\boldsymbol{r})) = -j\left(\frac{\varepsilon_r}{\mu_r}\right)^{1/2} \left(\frac{\varepsilon_0}{\mu_0}\right)^{1/2} \cdot \sum_{\mu=1}^{N} [c_\mu \boldsymbol{N}_\mu^1(k'\boldsymbol{r}) + d_\mu \boldsymbol{M}_\mu^1(k'\boldsymbol{r})]. \quad (8b)$$

The surface tangential fields $\boldsymbol{n} \times \boldsymbol{E}_+$ and $\boldsymbol{n} \times \boldsymbol{H}_+$ which appear in (7) are the source of the scattered field in the special problem as specified in (1). The scattered field in the special problem is the same as the scattered field in the complete problem (the application of the equivalence principle insured this), so the surface tangential fields $\boldsymbol{n} \times \boldsymbol{E}_+$ and $\boldsymbol{n} \times \boldsymbol{H}_+$ are the same fields in both the special problem and the complete problem. These tangential surface fields are in terms of the total external field evaluated at the surface. In the case of the complete problem, we can also write these in terms of the internal fields evaluated at the surface by applying the boundary conditions at the surface of the complete problem.

$$\begin{aligned} \boldsymbol{n} \times \boldsymbol{H}_+ &= \boldsymbol{n} \times \boldsymbol{H}_- \\ \boldsymbol{n} \times \boldsymbol{E}_+ &= \boldsymbol{n} \times \boldsymbol{E}_-. \end{aligned} \tag{9}$$

The plus (+) sign and minus (−) sign subscripts on the surface fields indicate that these fields are the total external and internal fields, respectively, evaluated at the surface. From (8), the tangential components of the internal fields evaluated at the surface are

$$\boldsymbol{n} \times \boldsymbol{E}_- = \sum_{\mu=1}^{N} [c_\mu \boldsymbol{n} \times \boldsymbol{M}_\mu^1(k'\boldsymbol{r}') + d_\mu \boldsymbol{n} \times \boldsymbol{N}_\mu^1(k'\boldsymbol{r}')] \tag{10a}$$

$$\boldsymbol{n} \times \boldsymbol{H}_- = -j\left(\frac{\varepsilon_r}{\mu_r}\right)^{1/2}\left(\frac{\varepsilon_0}{\mu_0}\right)^{1/2} \cdot \sum_{\mu=1}^{N} [c_\mu \boldsymbol{n} \times \boldsymbol{N}_\mu^1(k'\boldsymbol{r}') + d_\mu \boldsymbol{n} \times \boldsymbol{M}_\mu^1(k'\boldsymbol{r}')] \tag{10b}$$

and due to the equality of the tangential surface fields in (9), the expansions in (10) can be substituted into the first $2N$ of (7), giving a system of equations relating the unknown internal-field expansion coefficients to the known incident-field coefficients

$$\left[K + \left(\frac{\varepsilon_r}{\mu_r}\right)^{1/2} J\right] c_\mu + \left[L + \left(\frac{\varepsilon_r}{\mu_r}\right)^{1/2} I\right] d_\mu = -ja_\upsilon, \qquad \mu = 1,N \tag{11a}$$

$$\left[I + \left(\frac{\varepsilon_r}{\mu_r}\right)^{1/2} L\right] c_\mu + \left[J + \left(\frac{\varepsilon_r}{\mu_r}\right)^{1/2} K\right] d_\mu = -jb_\upsilon, \qquad \mu = 1,N \tag{11b}$$

where $\upsilon = 1,N$, and the I coefficients are given by

$$I = \frac{k^2}{\pi} \int_S \boldsymbol{n} \cdot \boldsymbol{M}_\upsilon^3(k\boldsymbol{r}') \times \boldsymbol{M}_\mu^1(k'\boldsymbol{r}')\, dS$$

while the J, K, and L coefficients have a similar form except for the cross products which are given by $\boldsymbol{M}_\upsilon^3 \times \boldsymbol{N}_\mu^1$, $\boldsymbol{N}_\upsilon^3 \times \boldsymbol{M}_\mu^1$, and $\boldsymbol{N}_\upsilon^3 \times \boldsymbol{N}_\mu^1$, respectively.

This set of $2N$-by-$2N$ simultaneous linear equations can be solved for the internal coefficients c_μ and d_μ. These can then be substituted into (8a) to find the electric field at any internal point ($\boldsymbol{M}$ and $\boldsymbol{N}$ are functions of θ, ϕ, and $k'r$ in the interior of the object).

The electric field can be determined at points of interest within dielectric objects with a real or complex dielectric constant. In the case of lossy objects, the distribution of volume power dissipation due to a specified incident field can be determined by calculating the quantity $\frac{1}{2}\sigma|E|^2$ at internal points of interest (σ here is conductivity as opposed to its use in (4) as a spherical harmonic index). The two features which will be studied here are the internal-field distributions and the absorption efficiency or normalized absorption cross section, which is given by

$$Q_{\text{abs}} = \frac{C_{\text{abs}}}{A} \tag{12}$$

where A is the geometric cross section of the body and C_{abs} is the absorption cross section which is equal to the total power absorbed divided by the incident power density S_i

$$C_{\text{abs}} = \frac{\frac{1}{2}\sigma \int_V |E|^2\, dV}{S_i}. \tag{13}$$

IV. Numerical Considerations

There are essentially three major operations involved in determining the internal electric field and thereby the absorption efficiency or other desired internal quantity. Given a specific dielectric object, the first step is to select an internal origin and numerically perform the surface integrations which are required to fill the coefficient matrix in (11). This procedure is accomplished by using a Bode quadrature technique [17]. The second step is to solve (11) for the internal-field coefficients c_μ and d_μ. This is accomplished by using a standard Gauss–Jordan algorithm. The third step then is to substitute the coefficients into (8a) to obtain the internal electric field.

The method of numerical solution for a particular problem consists of choosing a value for N (N is the maximum value of μ and υ and is a combined index incorporating the spherical harmonic indices σ, m, and n), solving the set of equations for the internal field, then repeating the calculation for successively larger N values until the final result in (8a) converges to a specified accuracy. The maximum value of N required for a given problem is dependent on the shape (deviation from a sphere), size, and dielectric constant of the object. Small spheres with a dielectric constant near unity require small values of N, while a large cylinder with relatively high index of refraction would require a much larger N value for solution. To reduce the numerical complexity, we consider only axisymmetric objects here. For axisymmetric objects, many of the cross terms involving σ (the even–odd index) drop out and, furthermore, it is possible to separate out the m dependence (azimuthal variation) so that rather than solving a $2N \times 2N$ system of equations once, it is possible to solve a much smaller $2n \times 2n$ system m times. This is equivalent to solving the problem for each azimuthal mode separately. This simplification carries through to the internal-field summation in (8a) so that the internal field can be broken down into separate summations over each azimuthal mode m. Each component summation

is summed over n and the total electric field is then found by summing up the individual fields due to each mode.

The validity of the numerical procedure was verified by making calculations for spherical bodies and comparing the results to those obtained by the Mie theory. Comparison was also made with low ka prolate spheroid calculations which were obtained using the long wavelength approximation [1]. Identical results were obtained in both cases. In all subsequent calculations, an ongoing validity test is made by first computing the internal field in an object with the mathematical origin of the problem located at the center of the object. The calculation is then repeated for the same object with the origin located off-center. This has the effect of making the physical problem appear to be different as far as the mathematics is concerned; however, the computer program must calculate the same internal field in either case.

V. Numerical Results

The equations from the previous sections have been programmed for solution on the University of Utah UNIVAC 1108, utilizing complex double precision arithmetic. Calculations have been made for a variety of objects characterized by a relative dielectric constant $\varepsilon_r = \varepsilon' - j\varepsilon''$ where $\varepsilon'' = \sigma/\omega\varepsilon_0$. The quantities which have been calculated are absorption efficiency versus the electrical size of the object (ka) and internal-field distributions at and about the resonant point. The absorption efficiency has been utilized rather than the absorption cross section so that it is not necessary to specify a particular σ and frequency. Combining (12) and (13) and defining

$$|E|^2_{\text{avg}} = \frac{\int_V |E|^2\, dV}{V}$$

gives

$$Q_{\text{abs}} = \frac{Bc\varepsilon_0\varepsilon''|E|^2_{\text{avg}}}{S_i} \tag{14}$$

where c is the speed of light and $B = \pi V/\lambda A = kV/2A$. Note that B is a function of the geometrical shape and (electrical) size of the object under consideration as well as the angle of incidence of the arriving wave (the geometric cross section A is a function of the angle of incidence). Fig. 4 shows the four shapes considered here and gives the factor B. Definitions of the angle of incidence and the polarizations of the arriving wave are also given.

In the case of the internal distributions, we plot $|E|^2$ rather than the internal power dissipation, making it unnecessary to specify particular values of σ and therefore frequency (we instead consider their ratio in ε'').

The purpose of the numerical calculations is to demonstrate the capabilities of the theoretical method in determining the salient features of the absorption characteristics of nonspherical objects. Rather than presenting results for a multitude of nonspherical geometrics, we instead focus our attention primarily on one shape, the prolate spheroid. We also show a few results for a finite cylinder and oblate spheroid.

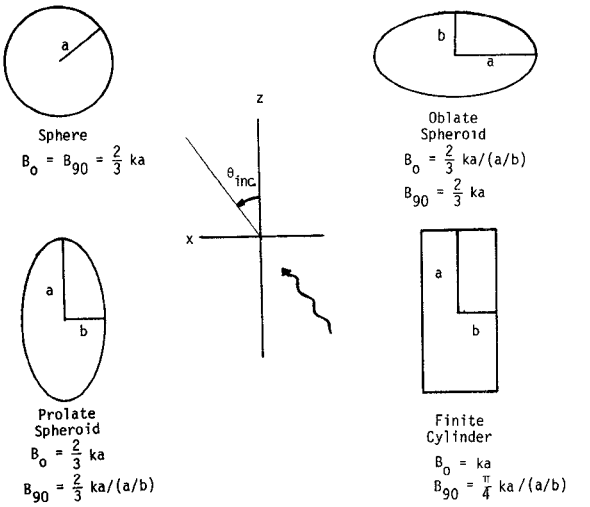

Fig. 4. Definition of geometrical bodies and corresponding factor B. The z axis is the axis of revolution and the angle of incidence is defined as shown. End-on incidence corresponds to $\theta = 0°$ and broadside incidence to $\theta = 90°$. The polarization of the incident wave is defined as either parallel or perpendicular to the x–z plane.

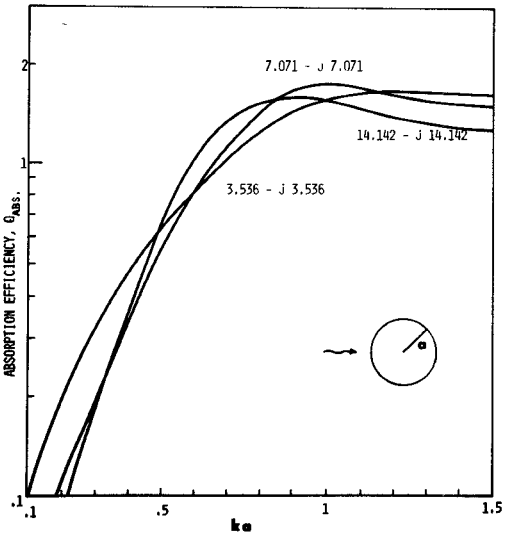

Fig. 5. Absorption efficiency versus ka for a lossy dielectric sphere.

To provide a reference point for comparison, we first show curves of absorption efficiency versus ka for a sphere. The resonance absorption characteristics of spheres have been studied extensively and reported in the literature [18], [19]. Fig. 5 shows the absorption by a sphere for three values of dielectric constant which are multiples of each other. The equality of the real and imaginary portions of ε_r is an arbitrary choice. Qualitatively, we see that the resonant ka point (the ka value giving maximum absorption) moves lower with increasing ε_r and we attribute this to the wavelength compression which occurs inside the sphere with increasing ε_r which increases the effective interaction volume, giving a higher loss at lower ka values. For ka values above the peak, minor oscillations may occur but the efficiency approaches a limiting value as ka increases. In the limit of large ka, we would expect the absorption and scattering efficiencies to sum up to an extinction efficiency of 2.

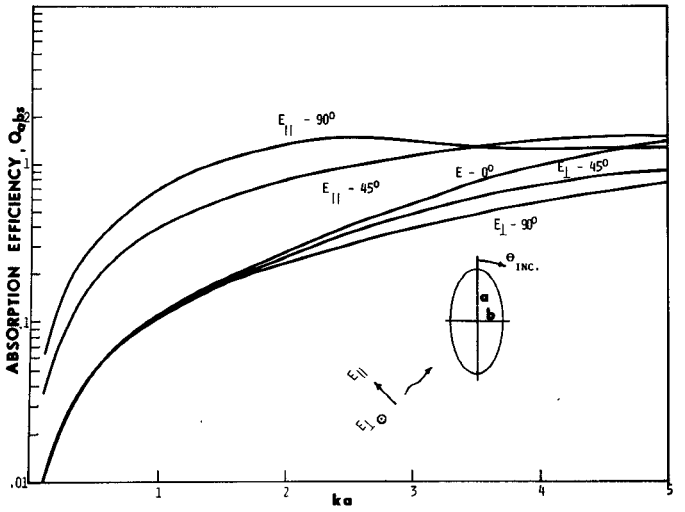

Fig. 6. Absorption efficiency versus *ka* for a lossy dielectric 6:1 prolate spheroid. Shows the absorption as a function of incident angle and polarization for *ka* values well beyond the first resonance. $\epsilon_r = 3.536 - j3.536$.

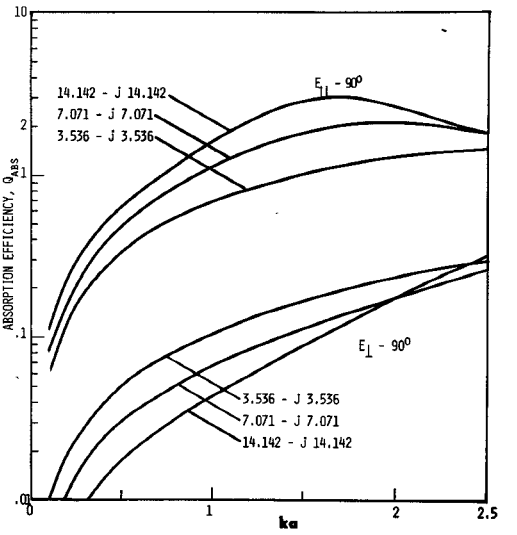

Fig. 7. Absorption efficiency versus *ka* for a lossy 6:1 prolate spheroid. Shows the effect of increasing dielectric constant for parallel and perpendicular polarizations.

Fig. 6 shows the absorption characteristics of a 6:1 prolate spheroid as the angle of incidence is varied from end-on to broadside. To allow observation of the absolute absorption behavior, all curves have been normalized to the geometric cross-sectional area corresponding to an angle of incidence of 90°. Some of the characteristics here can be explained by the similarity of the prolate spheroid to a dipole antenna. In the low *ka* region, the parallel polarized case shows a maximum for $\theta_{inc} = 90°$, while for higher *ka* the absorption at $\theta_{inc} = 45°$ becomes greater. This is not unexpected and is a result of the lobing effects seen in dipole antennas as the electrical length increases above a half-wavelength [20].

Although the effect is not as pronounced here as for a wire antenna, physically we note that the effective length seen by the $\theta_{inc} = 45°$ wave is less than the actual length by a factor of $\sqrt{2}$. This effective length is a major determinant of resonance, and therefore a higher *ka* is required for resonance at $\theta_{inc} = 45°$ than for the $\theta_{inc} = 90°$ broadside wave. For the $\theta_{inc} = 0°$ end-on wave, resonance is greatly dependent on the *kb* (= *ka*/6) dimension, and therefore the *ka* value required for resonance for end-on incidence is greater than that for the other two cases. An explanation of the absorption characteristics for the electric field parallel to the long axis of the spheroid based on the similarity of the prolate spheroid to a dipole antenna is useful; however, due to the large *b* dimension of the prolate spheroid relative to a wire antenna, an alternative explanation is also possible. For low values of *ka*, it has been shown [21] that the total absorption in a lossy dielectric can be considered as the sum of the power absorption due to coupling by the electric-field component of the incident wave and power absorption due to rotating electric fields (causing eddy currents) which is generated by the magnetic-field component of the incident wave. The explanation which has been developed based on a low *ka* theory would appear to account partially for the absorption characteristics noted here, even into the medium *ka* region.

Although the original explanation [21] was used to explain the coupling characteristics of spheres, it has also been used to describe low *ka* coupling to prolate spheroids [1]. Basically, the coupling of the electric-field component is greatest when the electric-field vector is mostly tangential to the surface and the magnetic-field coupling is greatest when the cross-sectional area perpendicular to the magnetic-field vector is greatest, i.e., the eddy-current coupling $\int \boldsymbol{E} \cdot \boldsymbol{dl} = j\omega\mu \int \boldsymbol{H} \cdot \boldsymbol{dA}$ is greatest. Therefore, the parallel polarized case at 90° incidence has maximum electric and magnetic coupling, the perpendicular polarized case at 90° incidence has minimum electric and magnetic coupling, and the zero-degree incident case has minimum electric-field coupling but maximum magnetic-field coupling. This qualitative explanation accounts for the relative absorption behavior in the low and mid *ka* ranges for the end-on and broadside cases. For 45° incidence, the power absorption for parallel and perpendicular polarizations falls between the corresponding curves for end-on and broadside incidence. At higher *ka* values this quasi-static explanation is no longer valid, and at the limit for which calculations have been made it appears that the absorption is becoming relatively independent of the orientation of the incident wave.

Fig. 7 shows the absorption characteristics of a 6:1 prolate spheroid due to a broadside incident wave for three different dielectric constants (which are multiples of each other) and two polarizations. Qualitatively, we note that in the parallel-polarized case, the *ka* value corresponding to maximum absorption decreases with increasing dielectric constant, which is similar to the sphere behavior exhibited in Fig. 5. Similar calculations have also been made for a 3:1 prolate spheroid and the increased polarization sensitivity in the 6:1 case is clear, i.e., the curves for parallel and perpendicular polarizations are farther apart than in the 3:1 case.

Comparing the parallel-polarization resonance (the lowest resonance) for prolate spheroids with different axial ratios, it has been noted that for a given dielectric constant,

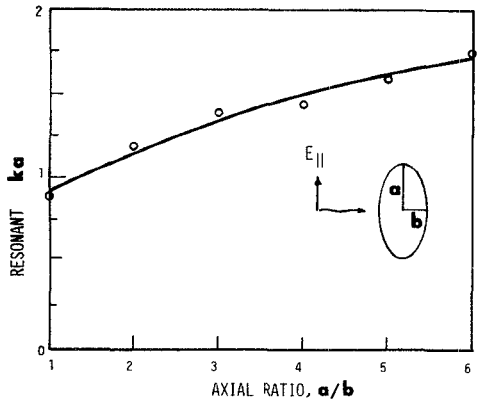

Fig. 8. Resonant ka versus axial ratio for a set of prolate spheroids with $\varepsilon_r = 14.142 - j14.142$. The circles are the resonate points as interpolated from an absorption efficiency curve for each spheroid. The solid line is the least squares fit.

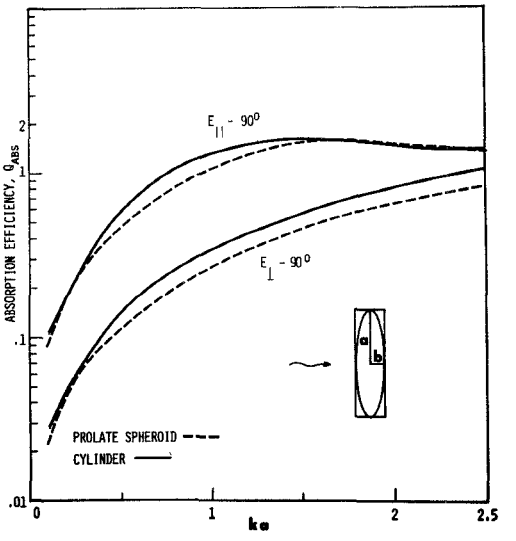

Fig. 9. Absorption efficiency versus ka for a lossy dielectric 3:1 finite cylinder and prolate spheroid with $\varepsilon_r = 3.536 - j3.536$.

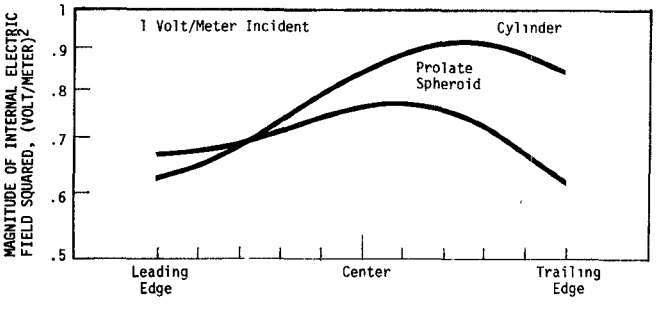

Fig. 10. Internal field $|E|^2$ distributions within a 3:1 prolate spheroid and cylinder at the approximate resonant point ($ka = 1.5$). Broadside incident wave.

the 6:1 spheroid resonates at a higher ka value than spheroids with lower axial ratios. Fig. 8 examines this behavior further by showing electrical length at resonance versus the a/b ratio for prolate spheroids where the incident wave is polarized parallel to the long axis. Note that for high-axial-ratio prolate spheroids, the resonant length is approaching an asymptote which is apparently independent of the a/b ratio. This behavior is related to the relative effect of the electric and magnetic coupling of the incident wave, which has just been described. Consider for a moment a set of prolate spheroids with the same a dimension and varying b dimensions. Using the arguments given earlier, for the case of 90° incidence we would expect maximum coupling of the parallel-polarized electric field for high a/b ratios where the tangential component of the electric field on the surface would be greatest. Resonance in this case would primarily depend on the total length of the spheroid being close to a multiple of a half-wavelength. For high a/b ratios, the coupling of the magnetic component of the incident wave is a minimum. For low a/b ratios, the electric-field coupling is less, but the magnetic-field coupling is greater (the cross-sectional area normal to the H-field vector is greater). If we think of the H-field coupling as due to closed loops about the H-field vector (eddy currents), then we would expect maximum coupling (resonance) when the circumference around the long dimension of the spheroid is an integral multiple of a wavelength (or equal to one wavelength for the first resonance). Setting the circumference around the long dimension of the prolate spheroid equal to a wavelength, the expression for resonant ka due to magnetic-field coupling of the incident wave is

$$(ka)_{\text{res}} = \sqrt{2/(1 + b^2/a^2)}.$$

Note that for a sphere this is unity and it saturates at $\sqrt{2}$ at high axial ratios. For low axial ratios, magnetic coupling appears to be the primary determinant of resonance giving away to E-field dominance at higher a/b ratios and this accounts for the increase in resonant ka with the axial ratio. For a perfectly conducting wire antenna, we would expect maximum electric-field coupling for the length equal to $\lambda/2$ or $ka = \pi/2 = 1.57$. It is clear that the curve in Fig. 8 is asymptotic to a value higher than this and this may be due to the relatively low conductivity of the prolate spheroid compared to a wire antenna.

Fig. 9 compares the absorption characteristics of a finite circular cylinder and a prolate spheroid, both objects having identical overall dimensions. The absorption characteristics of the two shapes are very similar and it would appear that the details of the shape are not critical in determining the absorption. Fig. 10 gives the internal-field distributions at $ka = 1.5$ (the approximate resonant point) for both the 3:1 prolate spheroid and the 3:1 circular cylinder. The internal-field distribution for the spheroid and cylinder are also very similar. One interesting feature here is that the field is greater on the backside of the cylinder than on the side upon which the incident wave strikes.

Fig. 11 gives the magnitude of the surface field around the major and minor dimension for the 3:1 prolate spheroid shown in Fig. 9. The capability of being able to determine surface fields should permit further understanding of the reactive-field energy-storage characteristics of dielectric objects, which is important in microwave-resonator applications. Although these curves simply show distributions along the surface in two directions, it would be quite easy to generate contour plots if we were interested in a detailed study of surface-field behavior.

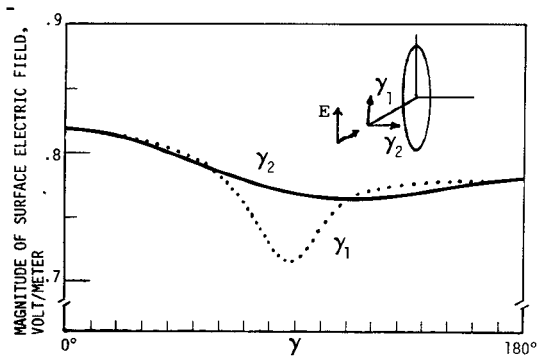

Fig. 11. Surface fields $|E|$ along the major and minor surfaces for the 3:1 prolate spheroid. $\varepsilon_r = 3.536 - j3.536$ and $k = 1.5$. Broadside incident wave, parallel polarization.

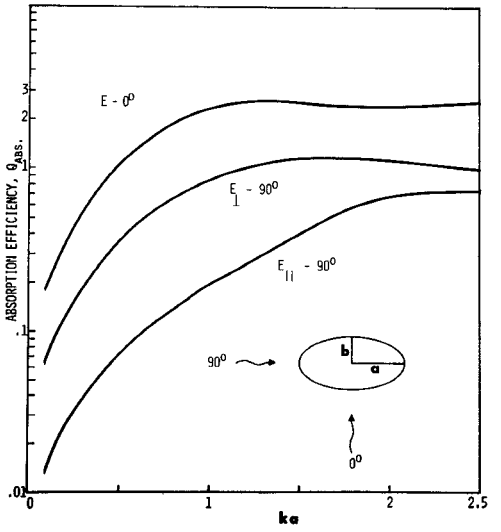

Fig. 12. Absorption efficiency versus ka for a lossy dielectric 3:1 oblate spheroid.

Fig. 12 shows the absorption efficiency for an oblate spheroid. Comparing this curve to corresponding curves for the prolate spheroid, we see that the earlier explanations of relative coupling and resonance frequency location also apply here. In particular, when the incident angle is zero degrees, the spheroid looks almost like a disk to the impinging electric field and therefore the electric-field coupling is very strong due to the large area of tangency. Using the previous arguments on the independent coupling of electric and magnetic components of the incident wave, we note that for end-on incidence, the magnetic-field coupling would be relatively weak, but the electrical-field coupling is so large that this case gives the maximum absorption. For broadside incidence with the electric field parallel, we have minimum electric and magnetic coupling and therefore minimum absorption. The electrical-field perpendicular case for this angle of incidence has medium electric-field coupling and large magnetic-field coupling giving a value of absorption lying between the other two cases.

Calculations have been made to determine the limitations of the numerical technique. Using a prolate spheroid model, ka and ε_r were increased until the origin off-center validity test showed that erroneous results were being generated.

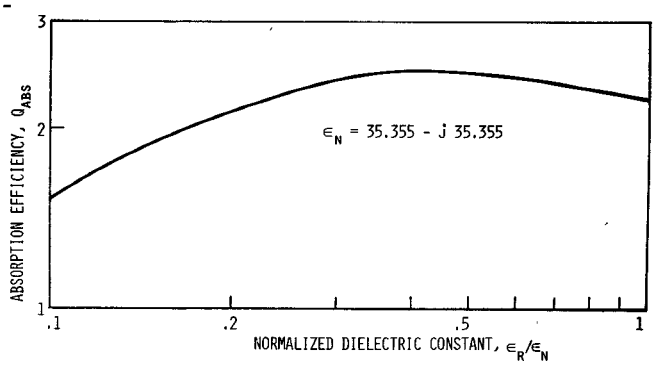

Fig. 13. Absorption efficiency versus ε_r for a 3:1 prolate spheroid. $ka = 1.5$. Broadside incident wave, parallel polarization.

When this occurred, the computer program was dissected to determine the mode of failure. It was found that the matrix associated with (11) becomes ill-conditioned with respect to matrix inversion and solution and that this ill-conditioning appears to be a function of the same variables which determine the matrix size required for convergence, i.e., the shape (deviation from a sphere), size, and dielectric constant. Ill-conditioning means that the solution vectors (in our case c and d) are very sensitive to small changes in the coefficients of the $(K\text{–}L\text{–}I\text{–}J)$ matrix and/or the right-hand side coefficients (a and b). It is an indication that the finite precision arithmetic available in the computer is not sufficient to differentiate the correct solution out of a range of solutions which satisfy the equations to the precision limits of the machine [22].

Given an object for which a numerical solution is not possible, it appears that of the physical characteristics that define the object (shape, size, and ε_r), that reducing the dielectric constant is most effective in restoring the condition of the matrix and thereby giving a solution. This indicates a possible means of extension of the envelope of cases for which the EBCM would be effective. Assume that one requires the solution for a given object for which a straightforward application of the EBCM gives an ill-conditioned system of equations. Then a set of calculations can be made for a series of reduced dielectric constants and a curve of Q_{abs} versus ε_r can be generated and used to extrapolate to the higher dielectric constant of interest. Fig. 13 shows such a curve for the 6:1 prolate spheroid at $ka = 1.5$. Note that the curve goes through a maximum which indicates a broad region where the absorption is relatively independent of ε_r. Also we note that the absorption efficiency can decrease or increase with a given change in ε_r, depending on which side of the peak we are operating. This technique has been employed to calculate the power absorption in muscle-tissue prolate-spheroid man models at VHF frequencies where the complex dielectric constant is typically on the order of a hundred.

VI. Conclusions

It has been shown that the EBCM can be used to determine the field within and on the surface of nonspherical dielectric objects during illumination by a plane electromagnetic wave. This information can be used to calculate

the absorption characteristics, maximum field points, or any other quantity desired. The theoretical technique as presented here is applicable to isotropic and homogeneous bodies. We have considered objects with a complex dielectric constant and have examined the dependence of the absorption efficiency on the nonspherical shape. The numerical limitations of the technique have been investigated and a method for extending the region of applicability has been indicated.

Acknowledgment

The author wishes to thank Prof. C. H. Durney and Prof. C. C. Johnson at the University of Utah and Prof. C. Yeh at UCLA for their helpful discussions and continuing interest throughout this research project.

References

[1] C. C. Johnson, C. H. Durney, and H. Massoudi, "Long wavelength electromagnetic power absorption in prolate spheroidal models of man and animals," *IEEE Trans. Microwave Theory Tech.*, vol. MTT-23, pp. 739–747, Sept. 1975.

[2] J. A. Morrison and M. J. Cross, "Scattering of a plane electromagnetic wave by axisymmetric raindrops," *Bell Syst. Tech. J.*, vol. 53, pp. 955–1019, July–Aug. 1974.

[3] P. Affolter and B. Eliasson, "Electromagnetic resonances and Q-factors of lossy dielectric spheres," *IEEE Trans. Microwave Theory Tech.*, vol. MTT-21, pp. 573–578, Sept. 1973.

[4] P. J. Wyatt, *Methods in Microbiology*, J. R. Norris and D. W. Robbins, Eds. New York: Academic, 1973, pp. 183–263.

[5] J. Van Bladel, "On the resonances of a dielectric resonator of very high permittivity," *IEEE Trans. Microwave Theory Tech.*, vol. MTT-23, pp. 199–208, Feb. 1975.

[6] ——, "The excitation of dielectric resonators of very high permittivity," *IEEE Trans. Microwave Theory Tech.*, vol. MTT-23, pp. 208–218, Feb. 1975.

[7] S. Asano and G. Yamamoto, "Light scattering by a spheroidal particle," *Appl. Opt.*, vol. 14, pp. 29–49, Jan. 1975.

[8] P. C. Waterman, "Symmetry, unitarity, and geometry in electromagnetic scattering," *Phys., Rev. D*, vol. 3, pp. 825–839, Feb. 1971.

[9] B. Peterson and S. Ström, "T-matrix for electromagnetic scattering from an arbitrary number of scatterers and representations of E(3)," *Phys. Rev. D*, vol. 8, pp. 3661–3678, Nov. 15, 1973.

[10] ——, "T-matrix formulation of electromagnetic scattering from multilayered scatterers," *Phys. Rev. D*, vol. 10, pp. 2670–2684, Oct. 15, 1974.

[11] P. W. Barber and C. Yeh, "Scattering of electromagnetic waves by arbitrarily shaped dielectric bodies," *Appl. Opt.*, vol. 14, pp. 2864–2872, Dec. 1975.

[12] D. S. Saxon, "Tensor scattering matrix for the electromagnetic field," *Phys. Rev.*, vol. 100, pp. 1771–1775, Dec. 15, 1955.

[13] S. A. Schelkunoff, *Electromagnetic Waves*. New York: Van Nostrand, 1943.

[14] R. F. Harrington, *Time-Harmonic Electromagnetic Fields*. New York: McGraw-Hill, 1961.

[15] J. A. Stratton, *Electromagnetic Theory*. New York: McGraw-Hill, 1941.

[16] P. M. Morse and H. Feshbach, *Methods of Theoretical Physics*. New York: McGraw-Hill, 1953.

[17] M. Abramowitz and I. A. Stegun, Ed., *Handbook of Mathematical Functions*. National Bureau of Standards, 9th printing, Nov. 1970.

[18] M. Kerker, *The Scattering of Light and Other Electromagnetic Radiation*. New York: Academic, 1969.

[19] D. J. Burr and T. L. Yuen, "Remote sensing of complex permittivity by multipole resonances in RCS," *IEEE Trans. Antennas Propagat.*, vol. AP-21, pp. 554–561, July 1973.

[20] H. Jasik, Ed., *Antenna Engineering Handbook*. New York: McGraw-Hill, 1961.

[21] J. C. Lin, A. W. Guy, and C. C. Johnson, "Power deposition in a spherical model of man exposed to 11–20 MHz electromagnetic fields," *IEEE Trans. Microwave Theory Tech.*, vol. MTT-21, pp. 791–797, Dec. 1973.

[22] P. A. Stark, *Introduction to Numerical Methods*. New York: Macmillan, 1970.